DOI: 10.13009/EUCASS2023-872
Aerospace Europe Conference 2023 – 10TH EUCASS – 9TH CEAS

Flexure-based gimbal with high support stiffness for rocket thrust vector control

Guillaume HUEBER ⋆† *and Jérémie HUSER* ⋆
⋆*EPFL*
Lausanne 1024 Switzerland
guillaume.hueber@epfl.ch · jeremie.huser@epfl.ch
†Corresponding Author

Abstract

In recent years, there has been increasing interest in the development of compliant mechanisms for use in aerospace applications. This paper presents the design, the theoretical model and testing of a compliant, high support stiffness two degrees of freedom gimbal prototype used for thrust vector control of a rocket engine. The design decisions taken to meet specifications are described. An analytical model is developed and compared to a pivot compression test. A final design of the gimbal assembly is prototyped.

1. Introduction

1.1 Thrust Vector Control

Thrust vector control (TVC) is a critical technology utilized in aerospace systems to maneuver and control the direction of thrust produced by engines. By dynamically altering the direction of the exhaust gases, TVC enables precise control of the vehicle's orientation, stability, and trajectory. This capability plays a major role in various vehicles, including spacecraft, rockets, and aircraft. These systems enhance maneuverability, improve mission flexibility, and enable advanced flight control strategies [1]. TVC mechanical systems are already extremely optimised and it seems to be difficult to improve the current designs (Fowler et al., 2011) [2]. Compliant mechanisms might be the key to view the problem from a different angle and change the classical approach of mechanical TVC systems.

1.2 Requirements

In a basic rocket, the vector force of the rocket nozzle is colinear with the center of mass of the rocket body. This doesn't create any torque around the center of mass. The idea behind thrust vectoring is to change the line of action of the rocket motor to control pitch and yaw. This allows to correct the rocket direction back to the desired orientation if needed. Thrust vectoring can be done in a few ways including additional "Vernier" thrusters, jet vanes or gimbaling the engine or nozzle [3]. Gimbals were chosen for this application as it's simpler for small scale tests. Gimballing the nozzle would have been simpler from a mechanical point of view; but this complicates the construction of the motor.

This is why this paper focuses on gimballing the whole engine. Our end goal is to integrate our gimbal with the rocket engine on a hopper vehicle. The latter would lift off the ground, sustain flight for a couple of seconds, move around and land back down. Our first tests are scheduled to be before the end of the year 2023. This research project, led by the EPFL Rocket Team, will help the team achieve a "space shot" exceeding the Karman limit (100km altitude) and be the first student group to achieve a landing using TVC by 2027. Our propulsion team at EPFL Rocket Team is working on a 1.2 kN thrust bi-liquid rocket motor engine to reach an altitude of 3 km. We will be using the same motor for our hopper. Thus, the gimbal mechanism shall mount the motor engine which is a cylinder with a diameter of 90 mm and a length of 240 mm. The motor has a mass of 9 kg. These large dimensions and weight impose a large moment of inertia. This influenced the choice of the position of the center of rotation which in turn influenced the choice of the design of the gimbal. The rest of the gimbal mechanism requirements can be found in Table 1.

1.3 State of the art

Compliant mechanisms simplify the design by reducing part counts, thus enhancing precision, reliability, and weight management, critical for aerospace applications. It eliminates the need for lubricants, increasing longevity during

DOI: 10.13009/EUCASS2023-872

Table 1: Gimbal Requirements

Description	Target value	Achieved value
Motor engine thrust load	1.2 kN	31 kN
Rotational range	±15 °	±26 °
Maximum mass	7 kg	6.3 kg
Time to reach 10° correction	100 ms	-
Resists peak axial acceleration	10 g	-
Resists peak lateral acceleration	3.5 g	-
Max operating temperature	150 °C	150 °C
Allows space for propulsion feed lines	Yes	Yes

extended space missions (Howell, 2001)[4]. A fully compliant space pointing mechanism has already been designed [5]. In addition to it being compliant, its monolithic construction allows to save weight and to have an equal coefficient of thermal expansion. It also has the advantage of having two actuators that can be attached to ground, reducing rotational inertia. A problem with this design is its relatively low support stiffness. It does sustain a thruster's load of 445 N but this system is mainly designed as a pointing mechanism on earth orbit satellites. While the design allows plumbing and wiring to pass through the mechanism, it doesn't allow the whole rocket engine to pass through. While this keeps the structure compact, it forces the center of rotation to be on the edge of the rocket engine or nozzle thus resulting in a higher rotational inertia requiring more torque from the actuator.

Compliant high support stiffness were considered (Naves et al.) [6]. Parallel stacked folded leafsprings allow a very high support stiffness and load capacity while still having a large range of motion. Another spherical flexure joint based on tetrahedron elements can sustain an incredible vertical load [7]. It has the advantage to have its center of rotation (CR) away from the structure, potentially having the CR at the center of mass (CM) of the rocket engine. The problem is the further away the CR is to the structure, the bigger the structure has to be. This makes it non suitable for this project. The disadvantage of these tools is that the CR would be on the edge of the rocket engine resulting in a higher rotational inertia. They also render difficult the space for propulsion feed lines.

2. Proposed mechanism

The main gimbal structure can be summarised as two pivots in series, one pivot for each axis. These pivots are doubled on each stage to divide the vertical load on each pivot by 2. By separating the main pivot into two, this allows the rocket engine to pass through the mechanism. The center of rotation can thus be located at the center of mass of the engine which has a much lower rotational inertia compared to having the CR at the edge of the engine. This allows a faster response time from the two actuators without a higher torque, which is critical in TVC systems. The fact that the engine can go through the mechanism also has the advantage of not risking damaging plumbing and wiring from pinching or shearing. Instead of having the second stage actuator moving with the first stage, the second stage actuator input was decoupled from the first stage. So both actuators can be connected to ground. This simplifies actuator mounting and lowers the rotational inertia of the first stage.

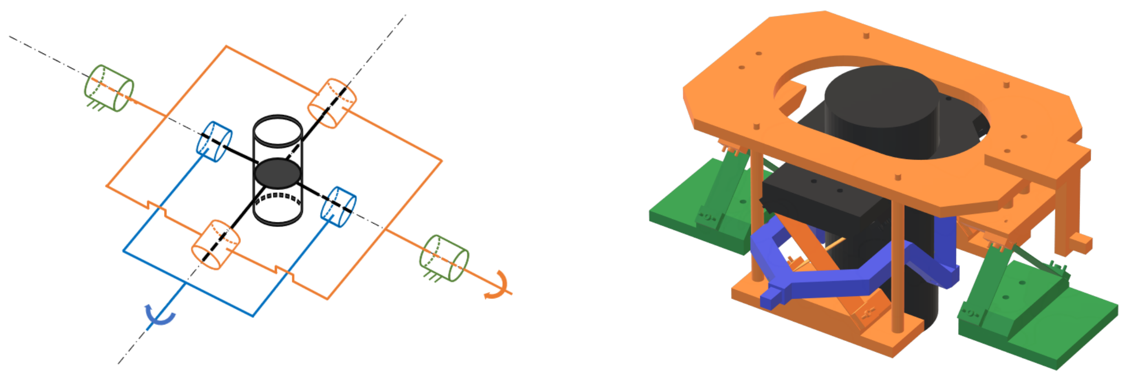

(a) Kinematic drawing of the gimbal mechanism

(b) Isometric view of the flexure-based gimbal design

Figure 1: Kinematic drawing and respective flexure-based isometric view of the gimbal design

DOI: 10.13009/EUCASS2023-872

The kinematic diagram of the system is shown in Figure 1a, the two blue cylinders representing the decoupling system. The bi-liquid rocket engine is represented by the black vertical cylinder in the center. The two green pivots are mounted onto the hopper structure. The green and orange kinematic pivots are transformed into compliant pivots, as illustrated in Figure 1b, which provides rotation in a defined range without friction. The blue pivots are modified into blades, working as decoupling pivots. There exist many different kinds of compliant pivots and our choice was clearly focus on having a high stiffness in the vertical axis and also on the ease of manufacturability. Flexure-based pivots which required the use of Electrical discharge machining (EDM) were therefore avoided due to cost. The cross-spring pivot was chosen for its simplicity, low rigidity and large range of motion. To achieve the actuator decoupling, a full cross spring pivot would work but its large size would increase the already large volume of the mechanism. The RCC pivot [8] would allow a smaller footprint but a simple flat spring works as well and has a lower stiffness.

The two different stages are shown in Figure 2. The decoupling system with the two flat springs is shown in Figure 3a. Finally, the assembly of the two stages as well as the decoupling system is shown in Figure 3b.

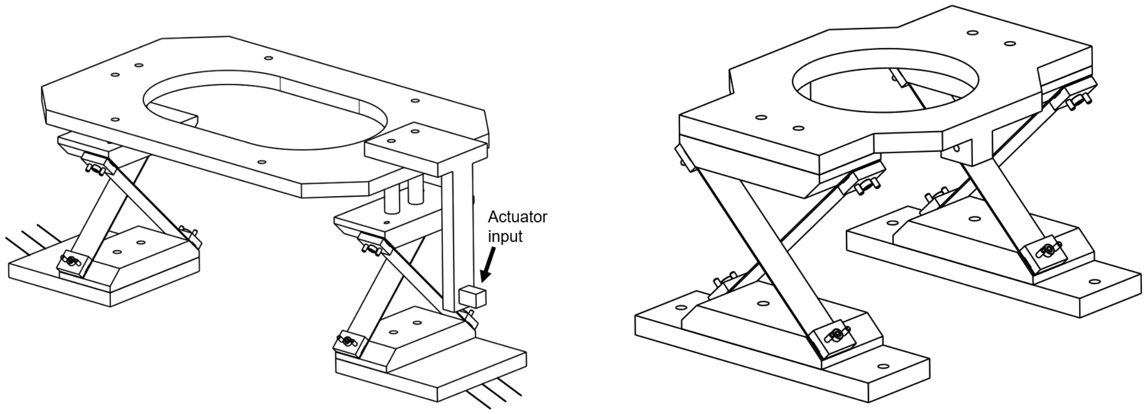

(a) First stage of the gimbal

(b) Second stage of the gimbal

Figure 2: Isometric view of the first and second stages of the gimbal mechanism

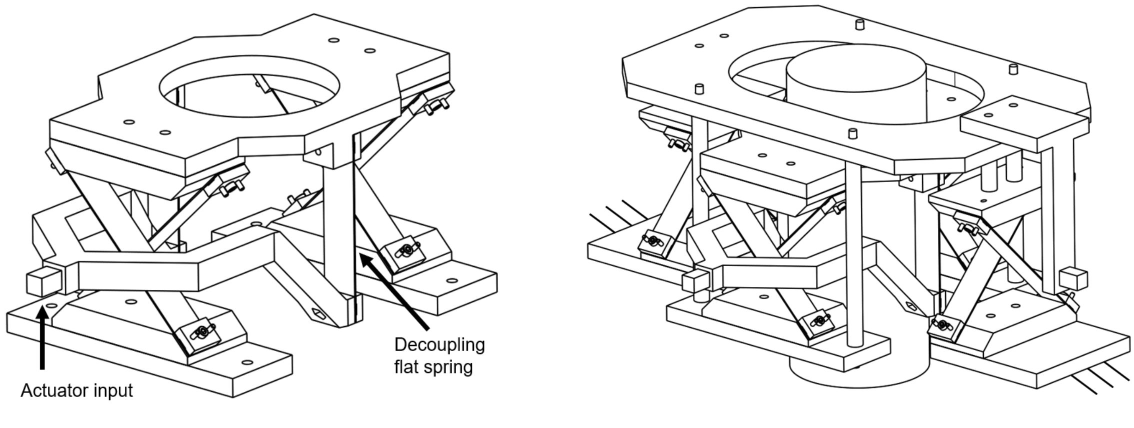

(a) Second stage with decoupling flat springs

(b) Assembly of both stages

Figure 3: Isometric views showing the decoupling system and the whole gimbal assembly

According to the theoretical model, pivots in compression lead to the flat springs buckling, leading to unwanted deformation of the pivot joint. Pivots in tension lead to flat springs subjected to tensile stress so no buckling takes place. The pivots can therefore sustain a greater load. This brought us to use a “traction-traction” system (Figure 4b) by adding a vertical member between the two stages. This leads to all pivots of the system being in traction, instead of a standard “traction-compression” (Figure 4a) system where one stage is in compression and the other is in traction. In Figure 4, the blue arrows represent compression forces and the green ones represent tensile forces. The drawings could suggest that there is a moment of force created by the load F but the real gimbal system is symmetric such that no moment is created.

DOI: 10.13009/EUCASS2023-872

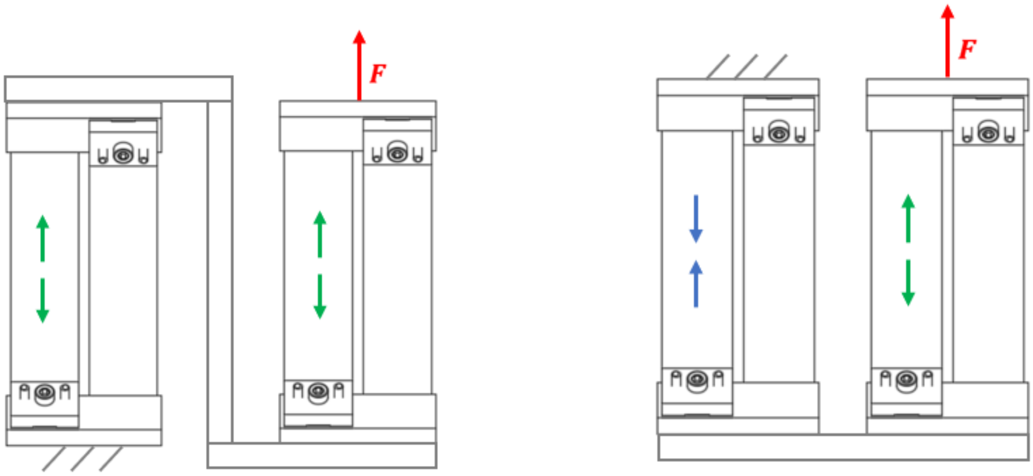

(a) Pivots in "traction-compression" (b) Pivots in "traction-traction"

Figure 4: Difference between the two stages being only in traction or in traction and compression

The mechanism showed in Figure 3b is not a monolithic construction. Indeed, to limit costs, it was chosen to assemble the gimbal mechanism. While this removes certain advantages of compliant mechanisms, the gimbal design can be modified to be manufactured by Electron Beam Melting (EBM) or Wire-EDM (Electrical Discharge machining).

3. Theoretical model

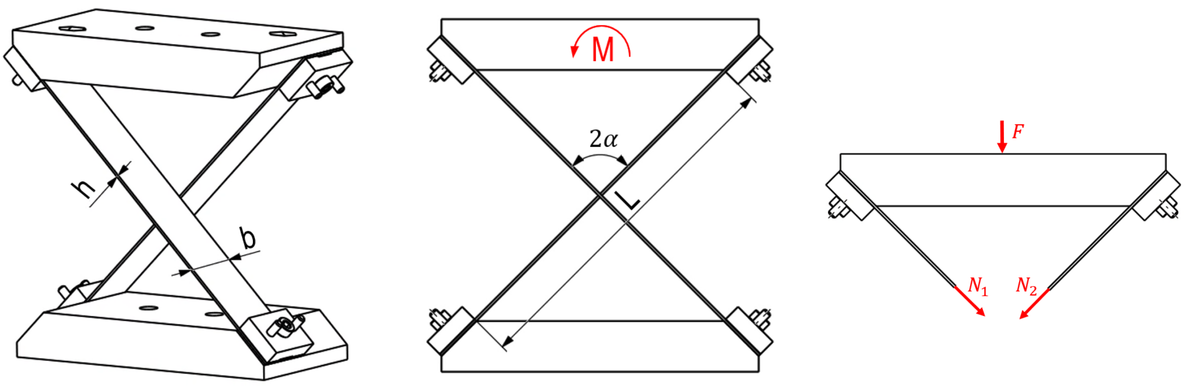

(a) Isometric view (b) Front view (c) Forces applied to the pivot

Figure 5: The cross spring pivot dimensions, applied load and internal forces

3.1 Single pivot: forces and stiffness

To model the maximum compressive and tensile load that can be applied to the pivot, the method of section was used to find out how much load is taken by each beam flexure. As the system is symmetric, the following equation can be derived: $N_1 = N_2$ with N the internal forces defined in Figure 6c. From the free body diagram and using Newton's first law of motion, the following equation can be derived $N_1 = N_2 = F/\sqrt{2}$. Knowing this and the Euler's critical load P_{cr} for buckling, the maximum compressive load on a cross spring pivto can be derived.

$$P_{cr} = \frac{\pi^2 \cdot E \cdot I}{(k \cdot L)^2} \tag{1}$$

DOI: 10.13009/EUCASS2023-872

With E the material's Young's modulus, I the second moment of inertia of the cross section of the beam, L the beam length and k the corrective length factor. As the beam is clamped on each end, the constant takes a value of $k = 1/2$ which greatly increases the buckling load. Using the definition of the dimensions of the beam established in Table 2, we also have $I = (bh^3)/12$. All of this brings us to the maximum compressive load F before buckling of:

$$F_{max,compression} = \frac{\sqrt{2} \cdot \pi^2 \cdot E \cdot b \cdot h^3}{3 \cdot L^2} \tag{2}$$

A similar calculation can be done for the tensile force expect we have to go up to the beam's failure instead of buckling. For this, the yield stress σ_y of the material is used to find the maximum internal force $N = \sigma_y \cdot b \cdot h$ in one of the beams. From this, we can find the maximum tensile load F of:

$$F_{max,tensile} = \sqrt{2}\sigma_y \cdot b \cdot h \tag{3}$$

If buckling doesn't take place first, the maximum load in compression will be the same load as $F_{max,tensile}$ considering the material to be isotropic. The material used for the flat springs is 1.4310 stainless steel as it is often used for the manufacturing of springs and other products requiring a good fatigue resistance [9]. Its material properties as well as the dimensions of the flat springs can be found in Table 2.

Table 2: Pivot dimensions and material properties

b[mm]	h[mm]	L[mm]	$I[10^{-13} \cdot m^4]$	E[GPa]	σ_y[GPa]	$\alpha[10^{-6} \cdot K^{-1}]$
20	0.7	100	5.72	185	1.6	16.8

These values can be plugged into (2) and (3) to find the maximum forces that one single pivot can support before failure: $F_{max,compression} = 590\,\text{N}$ and $F_{max,tensile} = 31.67\,\text{kN}$. From this, it's apparent why the traction-traction system was used. The requirements state that the gimbal mechanism must hold a rocket thrust of about 1.2kN.
According to Ref [8], the cross-spring pivot has the following rotational range before reaching the yield stress:

$$\theta_{adm} = \frac{2\sigma_{adm} L}{Eh} \tag{4}$$

With σ_{adm} the admissible stress we want to put the flat springs through. As the maximum amount of pivot cycles is desired, σ_{adm} was chosen to be the endurance (10^7cycles) stress of $\sigma_{adm} = 580MPa$ for our material. This gives us a rotational range of $\theta_{adm} = 51.3deg$ which gives a 70 % safety margin compared to the requirements' range.
According to Ref [8], the cross-spring pivot has the following angular stiffness:

$$K_\theta = \frac{2EI}{L} \tag{5}$$

As our displacement is under 45°, (9) can be used without a corrective factor. This means, one pivot of the mechanism has an angular stiffness of $K_\theta = 2.11\ [Nm/rad]$.
Since the pivot has one degree of freedom (DOF = 1), it can be found to have one degree of hyperstatism ($DOH = DOF - M$) as Grübler's formula for 3D systems [10] gives M = 0 :

$$M = \sum_{i=1}^{j} f_i - 6(j - N + 1) = 3 \cdot 2 - 6 = 0 \tag{6}$$

3.2 Decoupling system

The decoupling system allows both actuators to be connected to ground. It is made up of two flat springs shown in blue in Figure 6b. The system is shown in 3D in Figure 6a. These springs need a low lateral stiffness but a high vertical stiffness. This is to allow movement of the first stage without too much stiffness but also allow movement of the second stage without buckling the springs. The advantage of having two flat springs to achieve this is that, when rotating, one flat spring will be in tensile stress while the other will be in compressive stress. In this manner, if one spring starts to buckle, its length will be reduced. This will increase the traction force on the other and decrease the compressive force on the first one. The springs will nevertheless be sized to prevent buckling. Euler's critical load (1) can be derived to isolate the flat spring's thickness h_d:

DOI: 10.13009/EUCASS2023-872

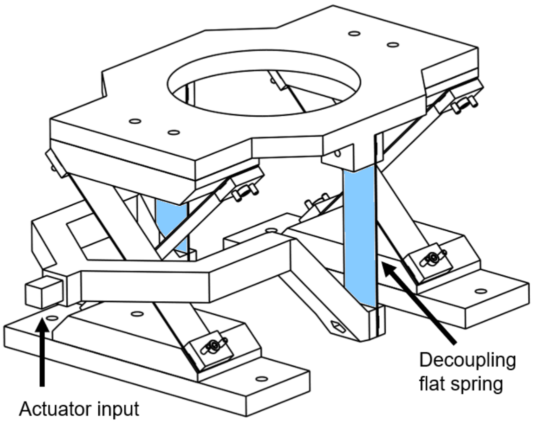

(a) Isometric view of the second stage with decoupling

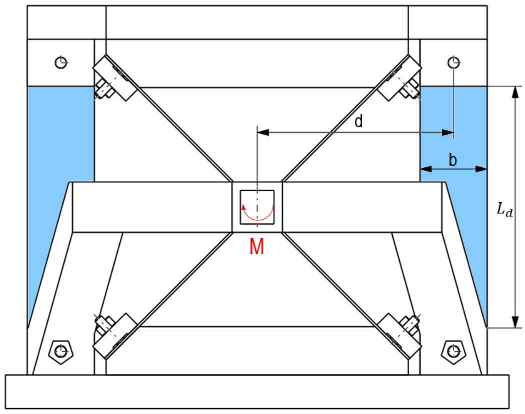

(b) Front view of the decoupling system with dimensions

Figure 6: Gimbal mechanism's second stage showing the decoupling system

$$h_d = \left(\frac{P_{cr}L_d^2}{4\pi^2 Eb}\right)^{1/3} \tag{7}$$

With $L_d = 72\ mm$ the free length of one of the decoupling springs. The force F_d needed to be supported by the flat spring is found considering the moment M generated by the actuator. As the middle of the spring is at a distance d from the actuator's axis, the force $F_d = M/d$. According to Ref [8], the following flat spring stiffness and rotational range can be found:

$$K_{\theta,M} = \frac{Ebh_d^3}{12L_d} \tag{8}$$

$$\theta_M = \frac{2\sigma L_d}{Eh} \quad or \quad \sigma = \frac{\theta_M Eh}{2L_d} \tag{9}$$

The dimensions found using (11) give a stiffness of $K_{\theta,M} = 0.115 Nm/rad$ for one spring and a stress of $\sigma = 345 MPa$ for the same deformation as the cross spring pivot giving a 40% margin of safety to the endurance ($10^7 cycles$) stress.

3.3 Main mechanism: Inertia and stiffness

For the mechanism's first stage, there are two decoupling flat springs as well as two pivots leading to a total of $K_1 = 4.45\, Nm/rad$. For the mechanism's second stage, there are just two pivots leading to a total of $K_2 = 4.22\, Nm/rad$. The decoupling system thus leads to a rigidity difference of only 5% between the two stages.
Knowing our displacement of $\theta = 15° = 0.262\ rad$, the torque required to achieve this displacement is equal to: $M_1 = 1.16\, Nm$. This is the static torque so it doesn't take into account the rotational inertia of the system and the rocket engine.

Rotational inertia was then computed using the aluminium plates' mass and the pivots mass and their relative distances to the corresponding axis of rotation. For the second stage, the rotational inertia is around $I_2 = 28\, kg \cdot mm^2$, and for the first stage, it was computed to be $I_1 = 103\, kg \cdot mm^2$. As this mechanism is in series, the difference of 3.7 times as much rotational inertia between the two stages was expected.

The whole gimbal mechanism has a high degree of hyperstatism, partly because the pivots and decoupling flat springs are doubled and partly because the cross spring pivots themselves are hyperstatic. Indeed, Grübler gives:

$$M = \sum_{i=1}^{j} f_i - 6 \cdot (j - N + 1) = 3 \cdot (8 + 2) + 2 - 6 \cdot (12 - 4 + 1) = -22 \tag{10}$$

With the joints being j = (10 flat springs + 2 actuators) and N = 4 being the number of bodies. The structure's degree of hyperstatism can then be found to be DOH = DOF - M = 24 with DOF = 2.

DOI: 10.13009/EUCASS2023-872

4. Experimental results

We did several tests such as compression, traction and stiffness tests to characterize the pivot.

4.1 Compression tests

For the following tests, we used the Zwick 100 kN uniaxial testing machine. It had a maximum force of 100kN and resolution of 1N. Compression tests aimed to determine the buckling limit of the pivot and therefore the minimal blade thicknesses required to support 600 N, which is half the maximum load stated in the requirements. Two pivots have to support a total force of 1.2 kN.

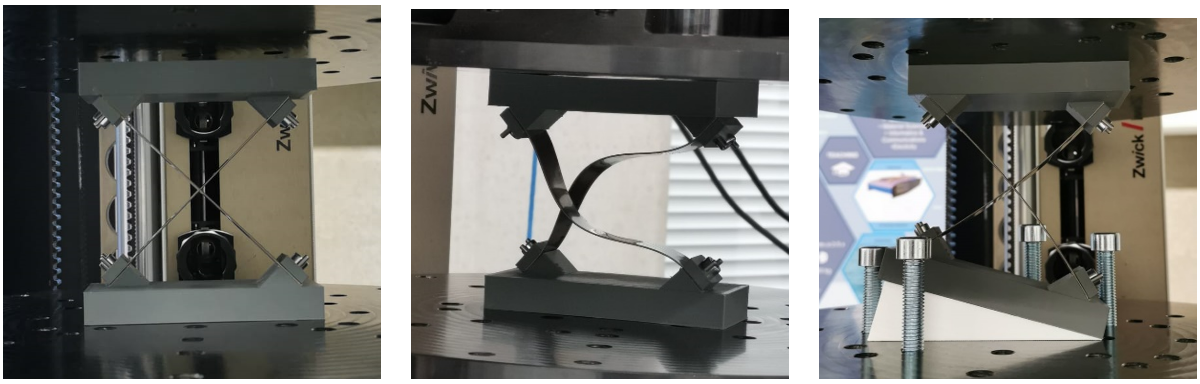

(a) Photo of the setup (b) Compressed and buckled pivot (c) Compression test with 15°of angle

Figure 7: The cross spring pivot dimensions, applied load and internal forces

The cross-spring pivot was tested in compression with 0.8 mm thick blades, and it was found that the pivot starts to buckle around 700 N (Figure 7b). This experimental value can be compared to the theoretical value:

$$F_{max,compression} = \frac{\sqrt{2}\pi^2 Ebh^3}{4\pi^2 Eb} = 881.4\,\text{N} \tag{11}$$

A difference arises due to the generation of a moment of force, which tends to rotate the pivot and bend the blades. This moment creates a stick and slip effect which is noticeable in Figure 8, where small peaks can be observed. In the gimbal design, two pivots operate in a mirrored configuration, which prevents such unintended rotation.

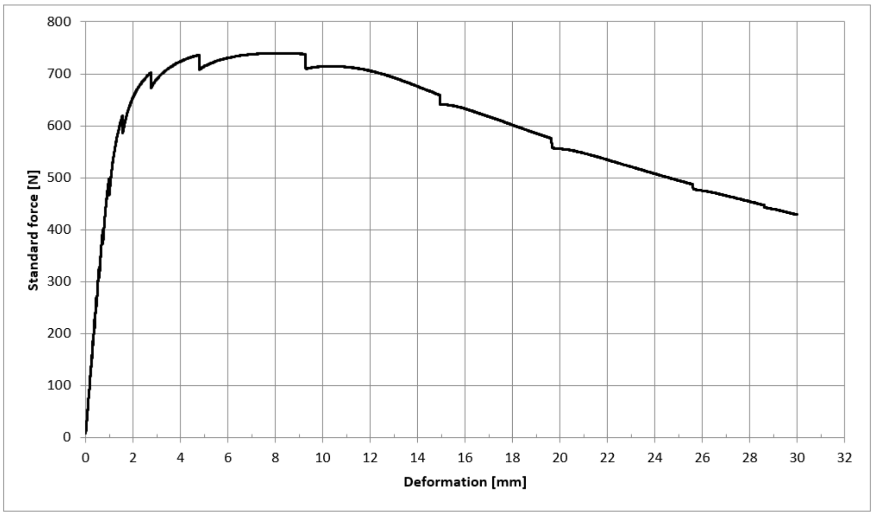

Figure 8: Compression test on a pivot with 0° of angle and 0.8 mm thick blades

We conducted an additional test to compare the compression of pivots at 0° and 15° angles, as illustrated in Figure 9. Our observations indicate that the pivot at a 15° angle undergoes more than 2.5 times greater deformation

DOI: 10.13009/EUCASS2023-872

compared to the 0° angle when subjected to a 600 N load which is the maximum load specified in the requirements for a single pivot.

Based on the conducted tests, we have reached the conclusion that a pivot operating in compression mode is not suitable for our application. This conclusion is primarily based on the significant deformations observed in the pivots, even when operating below the buckling limit and at 0° angle. For instance, a deformation of 2 mm is non-negligible. It is important to note that such deformations would generate stress on the actuators' axis, which is a critical factor we strive to minimize in our design.

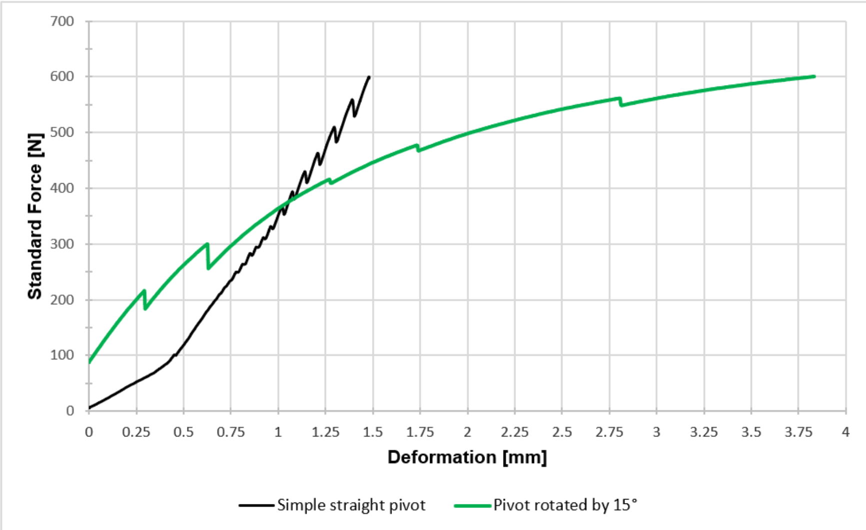

Figure 9: Compression test on a pivot with 0° versus 15° of angle

4.2 Rigidity test

Rigidity tests conducted manually using a dynamometer yielded an average angular rigidity of 2.58 Nm/rad, while the theoretical value is expected to be 2.11 Nm/rad. Although the tests were performed manually, resulting in slightly imprecise angles and values, the obtained rigidity values are still coherent.

4.3 Prototype

The prototype of our model, constructed using MDF and PETG materials, is shown in Figure 10. It has demonstrated an excellent decoupling system and guiding mechanism, enabling us to achieve a range of motion of over 15° in both axes. To further advance our project, the next step is to construct an aluminium version of the prototype in order to evaluate its performance.

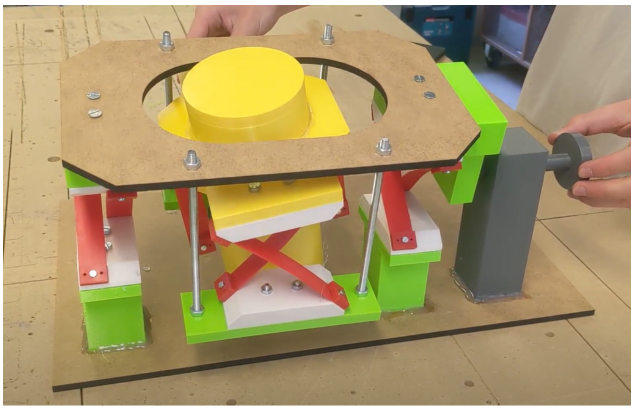

Figure 10: Prototype of the gimbal

DOI: 10.13009/EUCASS2023-872

5. Conclusion

We have described the design, modeling and development of a flexure-based gimbal used for rocket thrust vector control. The mechanism has a very high support load capacity allowing to theoretically sustain up to 31 kN. This is possible because the mechanism keeps the pivots in traction. The mechanism also allows large diameter engines to pass through, leading to several advantages including a lower rotational inertia and keeping the plumbing and wiring free from damage. The low rotational inertia allows a faster response time from the actuators which is crucial in TVC systems. The mechanism also allows a large amount of cycles at a large range of motion which is also crucial in space vehicles. The next step for us is to assemble a pivot with aluminium supports which will allow us to test it under traction before assembling the whole gimbal mechanism and proceeding to static fire tests of the rocket engine on the gimbal.

6. Acknowledgments

The authors acknowledge Loïc Tissot-Daguette and Hubert Schneegans for their insight and review of the report. Norbert Crot and Ivan Tomic were also helpful in machining the parts.

References

[1] Vidya Sagar Reddy. "The SpaceX Effect". In: *New Space* 6.2 (June 2018). Publisher: Mary Ann Liebert, Inc., publishers, pp. 125–134. ISSN: 2168-0256. DOI: 10.1089/space.2017.0032. URL: https://www.liebertpub.com/doi/full/10.1089/space.2017.0032 (visited on June 17, 2023).

[2] R. Fowler, Larry Howell, and Spencer Magleby. "Compliant space mechanisms: A new frontier for compliant mechanisms". In: *Mechanical Sciences* 2 (Oct. 20, 2011), pp. 205–215. DOI: 10.5194/ms-2-205-2011.

[3] *Rocket Control*. Mar. 7, 2011. URL: https://web.archive.org/web/20110307070030/http://microgravity.grc.nasa.gov/education/rocket/rktcontrl.html (visited on June 17, 2023).

[4] Larry L. Howell. *Compliant Mechanisms*. Google-Books-ID: tiiSOuhsIfgC. John Wiley & Sons, Aug. 3, 2001. 484 pp. ISBN: 978-0-471-38478-6.

[5] Spencer Magleby et al. "Monolithic 2 DOF fully compliant space pointing mechanism". In: *Journal of Mechanical Sciences* 4 (Dec. 2, 2013), pp. 381–390. DOI: 10.5194/ms-4-381-2013.

[6] M. Naves, R. G. K. M. Aarts, and D. M. Brouwer. "Large stroke high off-axis stiffness three degree of freedom spherical flexure joint". In: *Precision Engineering* 56 (Mar. 1, 2019), pp. 422–431. ISSN: 0141-6359. DOI: 10.1016/j.precisioneng.2019.01.011. URL: https://www.sciencedirect.com/science/article/pii/S0141635918307426 (visited on June 17, 2023).

[7] Jelle Rommers, Volkert van der Wijk, and Just L. Herder. "A new type of spherical flexure joint based on tetrahedron elements". In: *Precision Engineering* 71 (Sept. 1, 2021), pp. 130–140. ISSN: 0141-6359. DOI: 10.1016/j.precisioneng.2021.03.002. URL: https://www.sciencedirect.com/science/article/pii/S0141635921000726 (visited on June 17, 2023).

[8] Simon Henein. "Conception des structures articulées à guidages flexibles de haute précision". PhD thesis. Lausanne: EPFL, 2000. 226 pp. DOI: 10.5075/epfl-thesis-2194.

[9] *Cold-rolled, stainless spring steel strip 1.4310*. URL: https://www.brw.ch/en/cold-rolled-stainless-spring-steel-strip-1-4310-ts_59566101#SelectedPageSize=50&SelectedViewType=List&SelectedSorting=MY_SELECTION&SearchCategoryId=234 (visited on June 18, 2023).

[10] Martin Grübler. *Getriebelehre*. Berlin, Heidelberg: Springer, 1917. ISBN: 978-3-662-32126-3 978-3-662-32953-5. DOI: 10.1007/978-3-662-32953-5. URL: http://link.springer.com/10.1007/978-3-662-32953-5 (visited on June 18, 2023).